Hydrogen-induced ferromagnetism in ZnO single crystals investigated by magnetotransport

M. Khalid* and P. Esquinazi†

Division of Superconductivity and Magnetism, Institute for Experimental Physics II, University of Leipzig, D-04103 Leipzig, Germany

(Received 22 June 2011; revised manuscript received 13 March 2012; published 13 April 2012)

We investigate the electrical and magnetic properties of low-energy H^+-implanted ZnO single crystals with hydrogen concentrations up to ∼3 at% in the first 20-nm surface layer between 10 K and 300 K. All samples show clear ferromagnetic hysteresis loops at 300 K with a saturation magnetization up to ≃4 emu/g. The measured anomalous Hall effect agrees with the hysteresis loops measured by superconducting quantum interferometer device magnetometry. All the H-treated ZnO crystals exhibit a negative and anisotropic magnetoresistance at room temperature. The relative magnitude of the anisotropic magnetoresistance reaches 0.4% at 250 K and 2% at 10 K, exhibiting an anomalous, nonmonotonous behavior and a change of sign below 100 K. All the experimental data indicate that hydrogen atoms alone in the few percent range trigger a magnetic order in the ZnO crystalline state. Hydrogen implantation turns out to be a simpler and effective method to generate a magnetic order in ZnO, which provides interesting possibilities for future applications due to the strong reduction of the electrical resistance.

DOI: 10.1103/PhysRevB.85.134424 PACS number(s): 75.70.−i, 75.20.Ck, 75.30.Hx, 75.50.Pp

I. INTRODUCTION

Defect-induced magnetism (DIM) appears now to be a general phenomenon observed in nominally non-magnetic solids starting from the archetype graphite[1,2] to several oxides like ZnO, pure or doped with nonmagnetic elements,[3–8] HfO_2,[9] TiO_2,[10,11] $SrTiO_3$,[8,12] and SrO:N,[13] as well as Si-based samples,[14] to mention only a few examples of the large number being reported nowadays (for recent reviews on this subject see Refs. 15–18). Experimental facts demonstrate that defects, like vacancies, without or with the presence of nonmagnetic ad atoms, play a main role in triggering magnetic order in these systems. Recently, room-temperature ferromagnetism was reported in Cu-doped ZnO films, investigated by soft x-ray magnetic circular dichroism.[19] The results of this study strengthen the existence of the DIM phenomenon in general and in ZnO in particular.

ZnO is a wide-band-gap semiconductor, which crystallizes in the hexagonal wurtzite, zincblende, and rocksalt structures. However, hexagonal wurtzite is the most intensively studied crystal structure of ZnO because of its potential applications in the field of spintronics, transparent electronics, piezoelectricity, optoelectronics, etc. Hydrogen is one of the most abundant and unavoidable impurities in ZnO. The presence of hydrogen can influence the electrical and the magnetic properties of ZnO. The role of hydrogen in enhancing the ferromagnetism in 3*d*-transition-metal-doped ZnO was recently studied experimentally[20] and theoretically.[21] Note that, as shown in Ref. 19, the magnetic order is established between 3*d* elements via O vacancies of a similar concentration.[20] In Cu-doped ZnO, it is found that a long magnetic ordering is established between Cu ions via oxygen vacancies both with similar percentage concentrations.[19] Those authors showed with XPS and x-ray magnetic circular dichroism measurements that most Cu ions in ZnO are polarized and are present in Cu^{+1} and Cu^{+2} states. They proposed an indirect double-exchange model for the ferromagnetism in Cu-ZnO thin films.

On the other hand, there are theoretical studies reporting on the possibility of room-temperature ferromagnetism due to hydrogen adsorption at the surface of ZnO.[22,23] In contrast to 3*d*-metal-doped ZnO,[19–21] in this work we are interested in DIM in ZnO crystals triggered through the implantation of protons (H^+) at low energies and its influence on the magnetic and transport properties. Through the low-energy implantation we avoid a significant increase in the amount of other defects. The detailed experimental study presented in this paper demonstrates how the intentional doping of H^+, in the percentage range and at low enough energies, substantially influences the electrical and magnetic properties of the crystals. In particular, we show in this report a hydrogen-induced anisotropic magnetoresistance (AMR) as well as the anomalous Hall effect (AHE) in H-ZnO single crystals. Therefore, the existence of hydrogen-induced ferromagnetism in H-ZnO samples is supported not only by the usual magnetization data taken with a superconducting quantum interference device (SQUID)[24] but also by magnetotransport measurements. We note that there is a lack of experimental and theoretical studies on the possibility of hydrogen-induced magnetic order inside the crystalline structure of pure ZnO.

II. EXPERIMENTAL DETAILS

Hydrothermally grown ZnO (0001) single crystals of dimensions $(6 \times 6 \times 0.5)$ mm^3, with both sides polished, were supplied by CrysTec GmbH. The ZnO samples were exposed to remote hydrogen dc plasma at different time intervals in a parallel-plate configuration. The voltage difference between the two plates was kept at 1 kV. The samples were mounted on a heater block held at a fixed temperature of 400 °C and placed ∼100 mm downstream from the plasma with a bias voltage that provides 330 eV of implantation energy for H^+. A bias current of ∼50 μA was measured during the plasma treatment. The pressure in the chamber during the process was maintained at about 1 mbar. Three samples H-1, H-2, and H-3 for time intervals 30, 60, and 90 min, respectively, were treated in the H-plasma chamber. The implantation depth for the chosen energy as well as for the concentration characterization analysis (see below) was estimated using SRIM.[25] From this Monte Carlo simulation program we estimate a penetration depth of 20 nm

for the implanted hydrogen ions. As experimentally shown in Ref. 24 the main ferromagnetic signal comes from this near-surface region, in agreement with the estimates. The surface of ZnO surely plays a role in the ferromagnetic signal as shown in Ref. 8, but its contribution is much smaller than the one obtained after implanting a few percentage H^+ inside the first 20 nm near the surface region.

Nuclear reaction analysis (NRA) was used to determine the hydrogen concentration in ZnO crystals before and after hydrogen plasma treatment.[26] The NRA has a depth resolution of ∼5 nm with an average error in concentration of 0.02%. The hydrogen concentration in ZnO crystals measured by NRA before and after remote hydrogen treatment was found to be 0.14 ± 0.03 and 0.64 ± 0.07 at% in the first 200 nm from the surface, respectively.[27] From this concentration analysis we conclude that the first 20 nm near the surface region should have a hydrogen concentration of the order of ∼3 at% for sample H-3. The hydrogen concentrations for samples H-1 and H-2 are ∼1 and ∼1.8 at%, respectively.

We performed particle-induced x-ray emission (PIXE) measurements to analyze the concentration of magnetic and nonmagnetic impurities in the ZnO crystals. The penetration depth is $\sim 20 \cdots 30\ \mu$m for protons of 2-MeV energy. The impurity concentration (as micrograms element per gram ZnO) was Fe (<32), Co (<28), Ni (<34), Mn (<13), Cr (<)13, Ti (<21), and Ca (180 ± 20). There was no significant difference in these concentrations before and after H-plasma treatment. For crystals of the same batch, as in our case, no significant differences in the impurity concentrations between the crystals were measured.

The magnetization of the ZnO single crystals before and after the plasma treatment was determined with a SQUID. We estimate the mass magnetization assuming in all cases the same mass of 4 μg from the 20-nm upper surface region. The magnetotransport measurements were performed after the SQUID measurements in an Oxford cryostat with a magnetic field up to 8 T and a rotating sample holder allowing us to measure the resistance at different angles between the magnetic field and the input current direction. The electrical contacts on the samples were prepared using silver paste in a Van der Pauw configuration. The I/V characteristics were measured to check for deviations from the ohmic behavior. All the transport data presented in this paper were taken in a linear, ohmic regime. The resistance was measured with an ac resistance bridge with a relative resolution of 0.01%. The applied current was 10 μA.

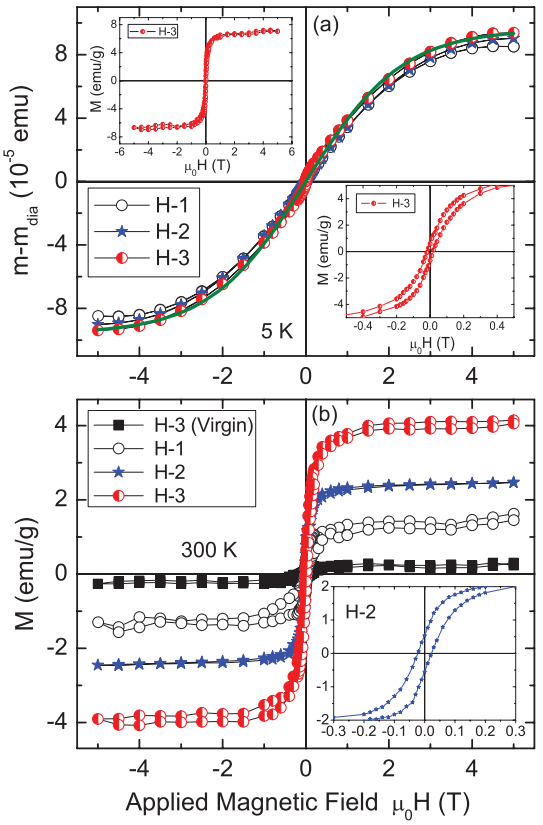

FIG. 1. (Color online) (a) Magnetic moment of the three H-ZnO crystals as a function of the magnetic field at 5 K. Insets: Ferromagnetic contribution for sample H-3 in two field ranges. This contribution is left after subtracting the linear diamagnetic and paramagnetic contributions from the total magnetic moment. The paramagnetic contribution is estimated with the Brillouin function [thick (green) line for sample H-3]. (b) Ferromagnetic magnetization of the same crystals along with the one from the H-3 virgin crystal at 300 K assuming a homogeneously distributed ferromagnetic mass in the first 20-nm near-surface region.[24] Note that the magnetic contribution of the virgin sample is subtracted from the one after H implantation for all three samples. The remaining difference is divided by the mass of a 20-nm surface layer (ferromagnetic mass). The weak ferromagnetic signal of the virgin sample (H-3) is also divided by the mass of a 20-nm surface layer in order to compare virgin and H-treated magnetizations.Inset: Hysteresis of the ferromagnetic part for sample H-2 at 300 K; one can recognize that the coercive field for this sample is ∼20 mT. Only a diamagnetic slope was subtracted from the data since the paramagnetic nonlinear contribution is negligible at this temperature. Note that the magnetization of H-ZnO crystals increases with H concentration.

III. RESULTS AND DISCUSSION

A. Magnetization measurements

Figure 1(a) shows the magnetic moment after subtraction of the linear diamagnetic contribution vs the applied field at 5 K for all three samples measured with the SQUID. The magnitude of the diamagnetic contribution in all three samples at 5 K was -3.21×10^{-8} emu/Oe. The subtracted diamagnetic susceptibility at 300 K for all samples was -3.26×10^{-8} emu/Oe, within a relative error of 1%. The magnetic data presented in Fig. 1(a) are composed of two further contributions. The main one, at 5 K, is paramagnetic and the magnetization follows the Brillouin function as $M = Ng\mu_B J B_J(\alpha)$ with $\alpha = g\mu_B JH/\kappa_B T$ (J is the total quantum orbital number, g the Landè factor, and k_B the Boltzmann constant). Taking the volume of the implanted 20-nm-thick H^+ layer, and from the paramagnetic fit [see Fig. 1(a)], we obtain a concentration of paramagnetic centers $NgJ \sim 10^{28}$ m^{-3}. Taking into account that we implant a few percentage H^+, we expect that some of these ions contribute as paramagnetic centers, and the rest to the magnetic order. In this case we expect the product $gJ > 2$. In fact, from the fit of the data of sample H-3 to the Brillouin function [green line in Fig. 1(a)],

we obtain $gJ = 3.4 \pm 0.2$. If one subtracts this paramagnetic contribution from the data, a ferromagnetic one remains, as shown in the insets in Fig. 1(a) for sample H-3.

At 300 K the paramagnetic contribution is negligible and the measured signal is given by the sum of the diamagnetic plus the ferromagnetic one from the near-surface region. After subtraction of the diamagnetic contribution, the magnetization coming from the ferromagnetic part was calculated assuming a ferromagnetic mass homogeneously distributed at the first 20-nm near-surface region. The ferromagnetic magnetization per total mass of a virgin, untreated ZnO crystal is of the order of 10^{-4} emu/g, similar to what has been reported for similar ZnO crystals.[8] For comparison and assuming that a 20-nm near-surface region in the virgin ZnO crystal is the source of the ferromagnetic signal, this would have a saturation ferromagnetic magnetization less than half that of sample H-1 [see Fig. 1(b)].

In Fig. 1(b) we see that the magnetization increases with H implantation as reported in Ref. 24 and it decreases with temperature; compare the results for sample H-3 with those taken at 5 K in the inset in Fig. 1(a). We would like also to note that the achieved ferromagnetic magnetization in pure ZnO thin films, prepared by pulsed laser deposition with a high vacancy concentration, is $\leqslant 10^{-2}$ emu/g,[7] i.e., smaller than the one we achieve with our implantation in the near-surface region. For our particular system (H-ZnO), SRIM simulations show that the implanted H concentration is about 8 orders of magnitude higher than the Zn- or O-vacancy concentrations[24] that one produces during implantation. The small atomic size of the implanted protons and the low implantation energy used allow basically defect-free implantation in ZnO.

All samples exhibit a coercivity of 18–20 mT at room temperature [see inset in Fig. 1(b)]. The saturation magnetization increases upon increasing the H concentration and reaches $\simeq$4 emu/g for sample H-3. The ferromagnetic magnetization at 5 K increases by $\sim$40% of its value at room temperature [see inset in Fig. 1(a)]. In Ref. 24 we showed that from the measurement of the temperature dependence of the remanent magnetic moment, we can estimate a Curie temperature of 450 ± 25 K for our samples.

Recently, Sanchez *et al.*[22] have theoretically shown that atomic hydrogen adsorbed on the Zn-ZnO (0001) surface can form strong H-Zn bonds and lead to a metallic surface with a net magnetic moment of $0.5\mu_B$ per H atom. The magnetization values obtained here indicate that our H-3 sample, for example, would have a net magnetic moment of $0.2\mu_B$ per hydrogen atom. This estimate is obtained taking into account the amount of H implanted. The difference between the two estimates may indicate that the assumed ferromagnetic mass (e.g., 20-nm thickness of a homogeneous ferromagnetic layer) is larger than the true one. This appears plausible because the hydrogen atoms are not necessarily homogeneously distributed inside the penetration depth. We believe that in the first 20-nm depth there are regions where the magnetic order is less developed and therefore one tends to overestimate the ferromagnetic mass. This picture of a rather inhomogeneous mixture of magnetic and nonmagnetic regions is of importance to interpret the transport data, as we discuss below.

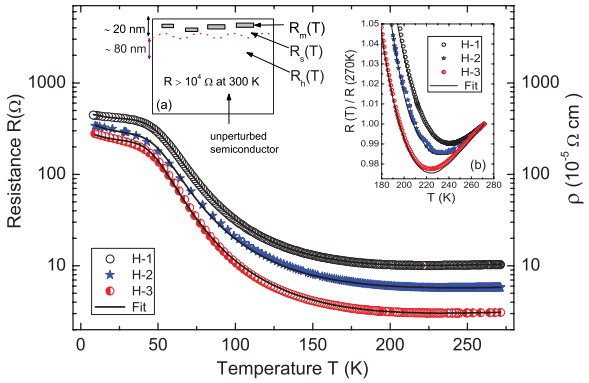

FIG. 2. (Color online) Resistance of the three H-ZnO samples as a function of temperature at a zero applied field. O the right y axis we show the resistivity estimated taking into account the 20-nm implanted thickness of the single crystal. Inset a: Sketch of the proposed model with the different regions and contributions necessary to understand the temperature-dependent resistance of H-ZnO single crystals. Inset b: Blowup of the high-temperature part where the resistance shows a qualitative change in its temperature dependence. The observed minimum shifts to low temperatures with increasing hydrogen concentration. Solid lines show the fits of the data to Eq. (2). Values obtained for R_1, R_2, and R_3 are $(0.015, 0.016, 0.018) \pm 0.001\ \Omega$, $(0.56, 0.55, 0.54) \pm 0.02\ \Omega$, and $(156, 160, 180) \pm 5\ \Omega$ for samples H-1, H-2, and H-3, respectively. Error bars indicate confidence limits. The rest resistance for all samples is $R_0 \leqslant 10^{-6}\ \Omega$.

B. Resistivity measurements

We measured the temperature dependence of the resistance of the three H-ZnO samples from 10 K to 270 K (see Fig. 2). The resistance decreases with increasing H concentration, therefore it is reasonable to assume that the resistivity of the implanted part is much lower than the resistivity from the rest of the single crystal, as has been reported.[28] This assumption is supported by the direct comparison of the estimated values of the resistivity—assuming conduction within the 20-nm implanted thickness (right y axis in Fig. 2)—with the resistivity of the virgin ZnO single crystal, which is at least 3 orders of magnitude larger already at room temperature.[29] From a comparison of the measured resistances for similar crystal geometries and electrode configurations,[29] it is clear that only the hydrogen-doped layer of the ZnO single crystal contributes significantly to the conductance, and not the remaining undoped part of the sample.

Before discussing in detail the observed behavior of the resistivity, we would like to describe briefly what is known about the hydrogen contribution to the formation and/or modification of the electronic band structure in ZnO. Hydrogen forms shallow donor states in bulk ZnO and is regarded as a source of n-type conductivity. These shallow donor states are formed approximately 30–60 meV below the conduction band. Upon reaching a certain doping level, the donor energy states can be dispersed into an impurity band because of the Coulomb fields arising from the compensating acceptors and ionized donors.[30] This impurity band can further split into two bands, i.e., a lower band I and an upper band I^-, which are formed with single-charged donors and neutral donors, respectively.[31,32]

As noted in Sec. III A, we assume that the implanted H^+ ions are not homogeneously distributed in H-ZnO samples. Then we may have hydrogen-rich metallic regions with resistance $R_m(T) = R_0 + R_1 T$, embedded in a doped semiconducting matrix with resistance $R_s(T) = R_2 \exp(\Delta E/2k_B T)$. R_0, R_1, and R_2 are free parameters as well as the activation energy ΔE, which is obtained by fitting the experimental data. Note that we consider a linear T dependence for the metallic part throughout the temperature range. The metallic region contributes mainly at high enough temperatures (see inset in Fig. 2), and therefore it is unnecessary to assume a more complicated T dependence that may be applicable at temperatures $T < 100$ K. We consider that these two contributions, metallic- and semiconducting-like, are in series (see sketch in Fig. 2). Due to the implantation distribution curve,[24] it is clear that below ~20 nm, a third intermediate region should exist that contributes with a resistance $R_h(T)$ in parallel to the other two. The best fits have been achieved by assuming a variable range hopping (VRH)-like mechanism as

$$R_h = R_3 \exp\left(\frac{E_{nn}}{T}\right)^{1/5}, \quad (1)$$

where R_3 is a free parameter and E_{nn} is a hopping energy. The total resistance is then given by

$$R(T) = [(R_h(T))^{-1} + (R_m(T) + R_s(T))^{-1}]^{-1}. \quad (2)$$

One can also take into account a fourth parallel resistance contribution arising from the pure ZnO single crystal below an ~200-nm-thick layer. However, the resistance of such a pure ZnO crystal at all temperatures is in the range of megaohms or higher, and therefore its contribution to the total measured resistance is negligible. The fittings to the data for the three crystals are excellent, as shown in Fig. 2. The activation energy obtained from the fittings for the three H-ZnO single crystals is $\Delta E = 60 \pm 2$ meV.

Qualitatively, the observed temperature dependence of the resistance is rather simple to understand. At temperatures below 50 K, the resistance of the semiconducting contribution R_s is higher than the resistance $R_h(T)$, the latter becoming the dominant transport path[33] because the thermal energy is not enough to excite the electrons from the upper impurity band I^- to the conduction band. The hopping energy obtained from the fitting of the experimental data is $E_{nn} \simeq 3 \pm 0.5$ meV. As the temperature increases the resistance of the H-ZnO samples decreases, following a semiconducting behavior with en effective activation energy $\Delta E \simeq 60$ meV. The larger the hydrogen doping, the lower is $R_m(T)$, and therefore the lower is the temperature of the minimum (see inset in Fig. 2). Although with this simple model we can understand qualitatively the behavior measured in the resistance as a function of the temperature and hydrogen concentration, it does not provide us with a clear hint about the regions that contribute to the magnetic signal. If the magnetic order is confined mostly within the first 20-nm surface region,[24] we expect that either the metallic or the semiconducting regions, or even an intermediate region between these two and the VRH part, contributes to the ferromagnetic signal. As the semiconducting contribution overwhelms the metallic one over a wide temperature range, it appears plausible that this one may be responsible for the magnetoresistance behavior we observe in H-ZnO single crystals.

C. Charge carriers

We performed Hall measurements in a Van der Pauw configuration in order to obtain the charge carrier density of our H-ZnO samples. Our Hall measurements confirm that the conductivity in H-ZnO single crystals is n type, as shown in Fig. 3. We note that the estimated carrier concentration is an effective one obtained using the simplest expression $n = 1/R_H e$, where R_H is the Hall resistance, assuming that only the sample volume of the first 20-nm H-rich surface layer of the ZnO single crystals contributes. In the case that electrons and holes contribute with different densities and scattering rates, we need to use the two-band model to obtain the carrier densities. The use of its equations, however, implies the introduction of free, unknown parameters, like the scattering rates. In order to facilitate the comparison of our data with literature values, we prefer to discuss the carrier density from the Hall data, stressing that the measurable quantity is R_H. The temperature dependence of the carrier density n is shown in Fig. 4.

The carrier concentration of samples H-1, H-2, and H-3 at room temperature is 6.72×10^{20}, 8.56×10^{20}, and 1.27×10^{21} cm^{-3}. These values are comparable to those found in, e.g., a Ga-doped ZnO system.[34] Above $T \sim 50$ K the carrier density increases with temperature, following the equation:

$$n = a + b \exp\left(\frac{\Delta E}{2k_B T}\right), \quad (3)$$

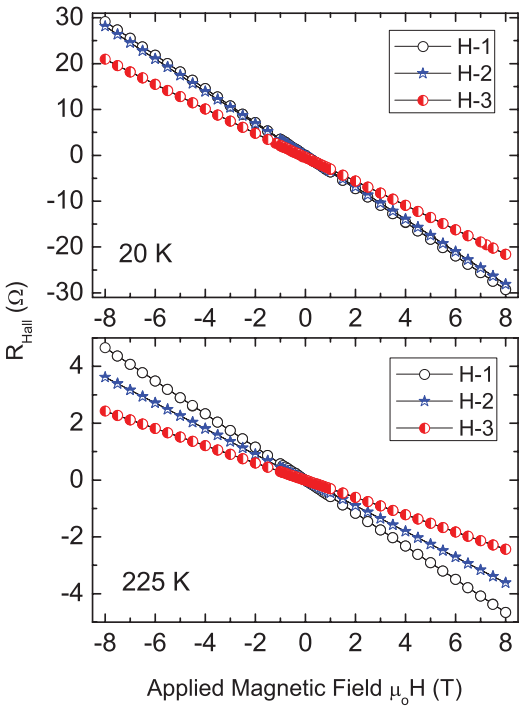

FIG. 3. (Color online) Hall resistance of H-1, H-2, and H-3 samples as a function of applied magnetic field measured at two temperatures.

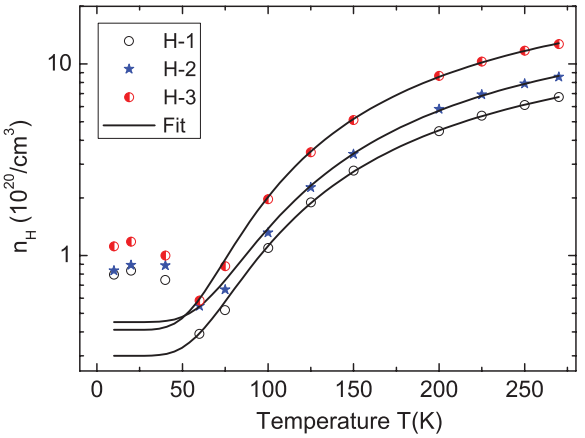

FIG. 4. (Color online) Carrier density of three H-ZnO single crystals as a function of temperature. The carrier density shows an anomalous behavior around ∼50 K. Solid lines are fits to the expression given by Eq. (3).

where a and b are free parameters. The activation energy obtained from the fits is $\Delta E = 60 \pm 2$ meV, in agreement with the activation energy values obtained from the resistivity measurements (see Fig. 2). As expected, the carrier concentration increases with the hydrogen concentration. The increase in n_H between the samples agrees roughly with the estimated increase in hydrogen concentration.

At temperatures $T \lesssim 50$ K, n increases with decreasing temperature (see Fig. 4). This is an anomalous behavior that appears to be related to the change of the main contribution to the measured resistance, i.e., from the semiconducting region above 50 K to the VRH one below it (see Fig. 2). In this case it might be that the simple relation to estimate n ($T < 50$ K) from the Hall resistance is not adequate and a more complicated equation for the Hall signal of a material with two contributions in parallel should be used.[35] We note that the anomaly at $T \sim 50$ K is observed in all magnetotransport properties we have measured, as we show in the following sections.

D. Magnetoresistance measurements

Apart from magnetization measurements, a further and important way to check for the existence of magnetic order is through the measurement of the magnetotransport properties. Unlike magnetization measurements, magnetotransport properties are much less sensitive to magnetic impurities, remaining below ∼0.1%. In this section we discuss the longitudinal magnetoresistance of H-ZnO where the magnetic field is applied parallel to the input current as well as to the sample main plane. The longitudinal magnetoresistance for the three H-ZnO samples measured up to 8 T at 10 K and 250 K is shown in Fig. 5. The magnetoresistance is defined as $\{[R(H) - R(0)]/R(0)\}$, where $R(H)$ and $R(0)$ are the resistances with and without an applied magnetic field, respectively.

All samples show a negative magnetoresistance at all temperatures and magnetic fields applied parallel to the main plane of the samples. Negative magnetoresistance has been observed in several other ZnO systems that show some kind of magnetic order.[36,37]

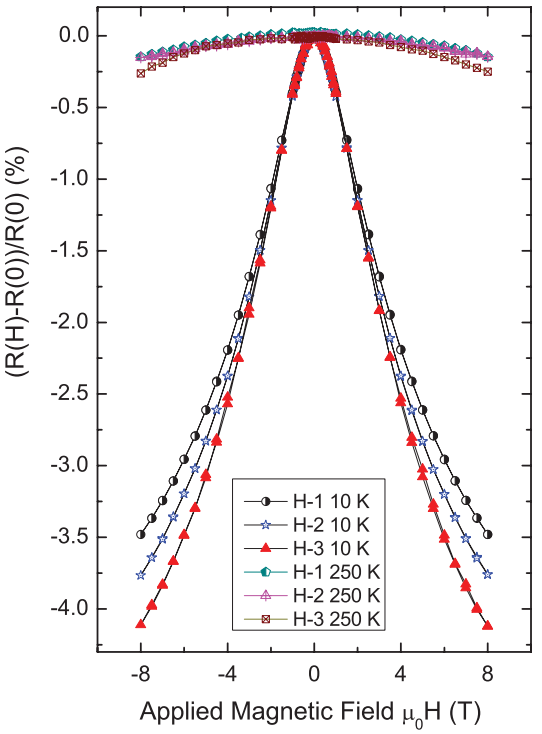

FIG. 5. (Color online) Magnetoresistance (in percentage) as a function of applied magnetic field at 10 K and 250 K for three H-ZnO samples. A clear correlation between magnetoresistance and H concentration is observed. Magnetoresistance increases with H concentration.

Figure 6 shows the temperature dependence of the magnetoresistance for the H-1 sample. Similar temperature-dependent magnetoresistance is observed for the other two samples. It is clear from Fig. 6 that the magnetoresistance of H-ZnO decreases in general with temperature. However, its field curvature at $T \sim 50$ K changes, and from 50 K to 75 K the magnetoresistance increases with temperature. The decrease in the magnetoresistance with temperature is expected because the magnetization at saturation of these samples also decreases with temperature (see Fig. 1). As we have observed in the carrier concentration, the anomalous behavior of the magnetoresistance around 50 K might be related to the change of the main contribution to the resistance. Taking into account that the main contribution to the magnetic signal comes from the 20-nm surface contribution, the VRH part and the magnetic semiconducting part might have a common interface, which shows magnetic order and contributes to the magnetoresistance at low temperatures.

To elucidate our experimental results for the magnetoresistance, we use a model proposed by Khosla and Fischer[38] that combines negative and positive magnetoresistances in semiconductors taking into account a third-order expansion of the s-d exchange Hamiltonian. The semiempirical formula is

$$\frac{\Delta\rho}{\rho_0} = -a^2 \ln(1 + b^2 B^2) + \frac{c^2 B^2}{1 + d^2 B^2}, \qquad (4)$$

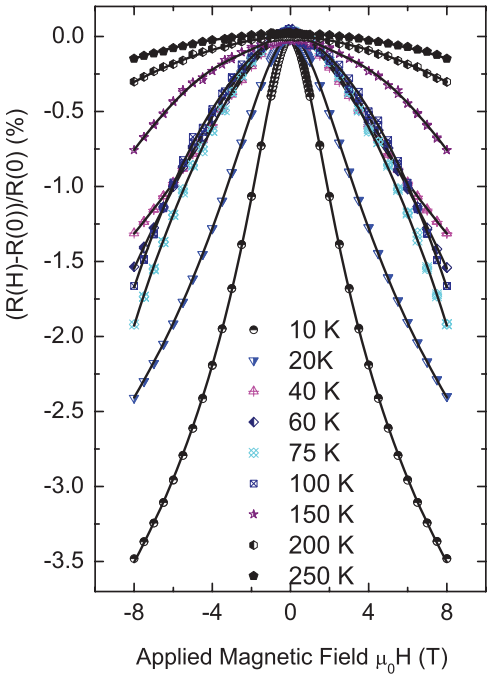

FIG. 6. (Color online) Magnetoresistance of sample H-1 (the other two samples show a similar dependence) as a function of applied magnetic field measured at several temperatures. The magnetoresistance shows a negative temperature dependence, but with an anomaly around 50 K. Solid black lines through the data points are fits to Eq. (4).

where c and d are parameters that depend on the conductivity and the carrier mobility, respectively. We consider these to be free parameters. The other two parameters are given by

$$a^2 = A_1 J\rho_F [S(S+1) + \langle M^2 \rangle], \tag{5}$$

$$b^2 = \left[1 + 4S^2\pi^2 \left(\frac{2J\rho_F}{g}\right)^4\right] \frac{g^2\mu^2}{(\alpha kT)^2}, \tag{6}$$

where μ is the mobility and α is a numerical constant. The parameters a and b in Eq. (4) depend on several factors such as the spin scattering amplitude A_1, the exchange integral J, the density of states at the Fermi energy ρ_F, the spin of the localized magnetic moments S, and the average magnetization square $\langle M^2 \rangle$. The negative first term in Eq. (4) is attributed to a spin-dependent scattering in the third-order s-d exchange Hamiltonian, while the positive part [second term in the expression of Eq. (4)] takes into account field-induced changes due to the two, s and d, conduction bands with different conductivities.

The fits of the experimental data to Eq. (4) are shown in Fig. 6. The data can be well fitted with this model at all measured temperatures. All four fitting parameters show different temperature dependences (see Fig. 7). Note that the positive magnetoresistance in our samples is compensated by the large negative magnetoresistance contribution. Therefore, the uncertainty of the parameters c and d is rather large because they are not independent of the fitting procedure. Therefore, we concentrate on the negative scattering contributions a and b. The fitting parameter b for the three H-ZnO samples is plotted as a function of inverse temperature in Fig. 7(b). The

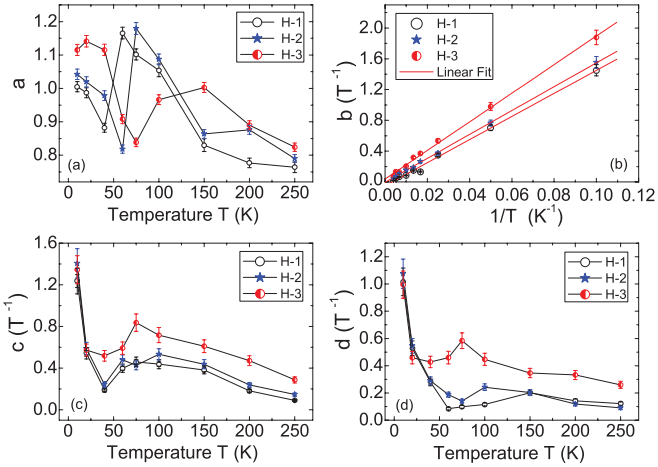

FIG. 7. (Color online) Temperature dependence of the fitting parameters a, b, c, and d of three H-ZnO samples.

parameter b shows a linear dependence, in good agreement with theory. We found that the parameter a is almost temperature independent and increases with H concentration in the temperature range 50 K $\geqslant T \geqslant$ 100 K, indicating that the sample with a higher H concentration (H-3) is more magnetic, in agreement with the SQUID data shown in Fig. 1.

Parameters a and b, defined in Eqs. (5) and (6), respectively, are used to obtain the values of $J\rho_F$ and A_1. The values of $J\rho_F$ and A_1 obtained from the experimental data are 0.56 and 0.14 for $S = 1/2$ and $\mu = 36$ cm^2/V s at 10 K, respectively. The values of $J\rho_F$ and A_1 for $S = 3/2$ are 0.33 and 0.12, respectively. The value of $J\rho_F = 0.33$ for $S = 3/2$ in H-ZnO is similar to the one obtained in the CdS system $J\rho_F = 0.4$.[38] These results strongly suggest the contribution of s-d interaction in the H-ZnO system. We may now ask whether it is reasonable to assume that the studied system has d conduction electrons. An answer to this question comes at the end of the next section.

E. Anisotropic magnetoresistance

There are two other magnetotransport effects that are observed in our H-ZnO crystals and are worth mentioning. One of them is the AMR effect. This effect represents the change in the resistance of a ferromagnetic material with the angle between the input current and the applied field in plane. It is commonly associated with the presence of a spin splitting of the electronic band at the Fermi level and a finite spin-orbit (L-S) coupling. The AMR arises in second order in the L-S coupling, in contrast to the magnetocrystalline anisotropy. In ferromagnetic materials with s and d bands, AMR is understood, arguing that the spin-orbit scattering increases the resistance by allowing a spin-flip and, through this, the occupation of free d states in the corresponding spin-dependent band. In general it is expected that the resistance is higher when the applied field is parallel to the current. We define the AMR amplitude as

$$\Delta R/R_{\text{avg}} = \frac{|R(H_\parallel) - R(H_\perp)|}{(R(H_\parallel) + R(H_\perp))/2}. \tag{7}$$

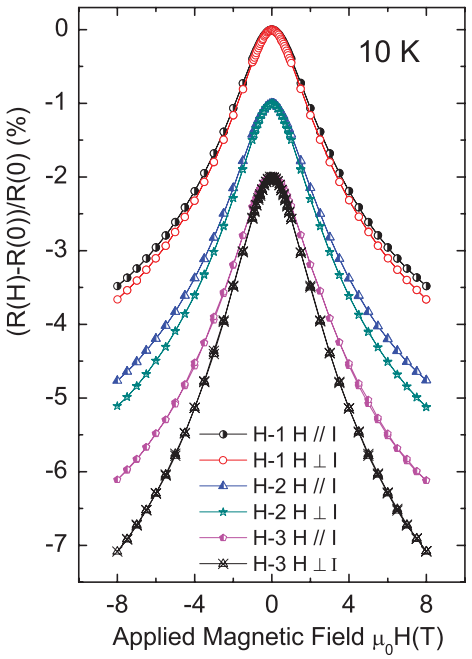

FIG. 8. (Color online) Magnetoresistance of H-ZnO samples at 10 K for two configurations of angles between the current and the applied magnetic field. For clarity, the data curves for samples H-2 and H-3 are shifted by a constant value.

For polycrystalline ferromagnetic samples the change in the resistance due to the AMR has the following angle dependence:

$$\frac{\Delta R}{R(H=0)} = A\cos^2\theta, \tag{8}$$

where θ is the angle between the current I and the applied field or magnetization direction (in saturation) and A is a constant that depends on the density of d states at the Fermi level, on the magnetization, and on the sample quality.

Figure 8 shows the field dependence of the magnetoresistance for $\theta = 0^\circ$ and 90° at 10 K for three H-ZnO samples. The angle θ is the angle between the applied current and the magnetic field. We observe a clear AMR effect in the three H-ZnO samples. We note that the AMR effect was already measured in ZnO, but doped with Co.[39] Our results show clearly that a fundamental property of ferromagnetic materials such as the AMR can also be obtained by DIM in an oxide. The AMR effect in H-ZnO single crystals increases with H concentration (see Fig. 8).

However, for ferromagnetic single-crystalline systems some influence from the lattice anisotropy can be expected in the AMR, and in this case the angular-dependent magnetoresistance is described by a Fourier series of $\cos(n\theta)$ and $\sin(n\theta)$ as

$$\frac{\Delta R}{R(H=0)} = \sum_{n=1}^{n=\infty} s_n \sin(n\theta) + \sum_{n=1}^{n=\infty} c_n \cos(n\theta), \tag{9}$$

where the coefficients s_n and c_n are related to the Hall and magnetoresistance contributions in the system.

In order to study the AMR in more detail, we measured the angular magnetoresistance at a constant field of 5 T at several temperatures (see Fig. 9). The variation of the angle

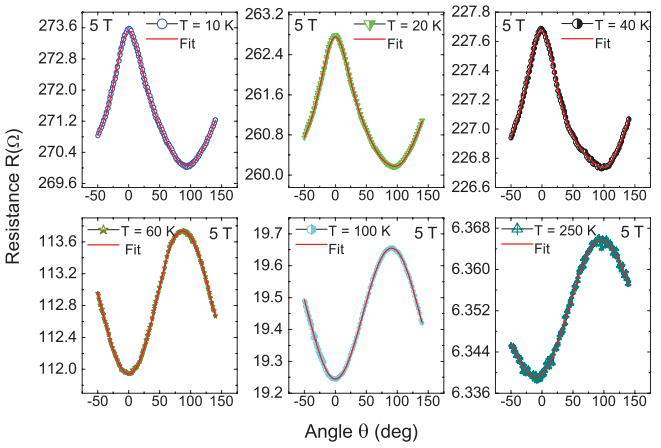

FIG. 9. (Color online) Angular magnetoresistance of sample H-1 at a constant field of 5 T at several temperatures. Solid (red) lines are fits to the experimental data following Eq. (9).

between the magnetic field and the current ranges from -50° to 140°. This range of angle is necessary because we expect a 180° periodicity. There are several distinct features in the experimental data shown in Fig. 9. (i) At $T < 50$ K the AMR is higher at $\theta = 0^\circ$ (field and current parallel to each other) than at $\theta = 90^\circ$, in agreement with the usual behavior. (ii) At temperatures $T > 50$ K the AMR changes sign (or it shows a 90° shift in the angle dependence; see Fig. 9). (iii) Figure 10 shows the AMR amplitude [see Eq. (7)] as a function of temperature for the three samples. There is a clear anomalous increase with temperature between 50 K and 100 K, despite the fact that the magnetization at saturation decreases monotonously over the whole temperature range according to the SQUID measurements (not shown). Note that the magnitude of the AMR in our H-ZnO samples at 250 K is ~0.4%, a value comparable to the AMR observed in, e.g., Co films[40] and Co:Cu multilayered nanowires.[41] (iv) The measured angle dependence does not follow Eq. (8), applicable for polycrystalline materials, and indicates that the magnetic contribution in our H-ZnO single crystals comes from a single crystalline phase after H-plasma treatment. The AMR curves obtained for all three H-ZnO samples are fitted by Eq. (9)

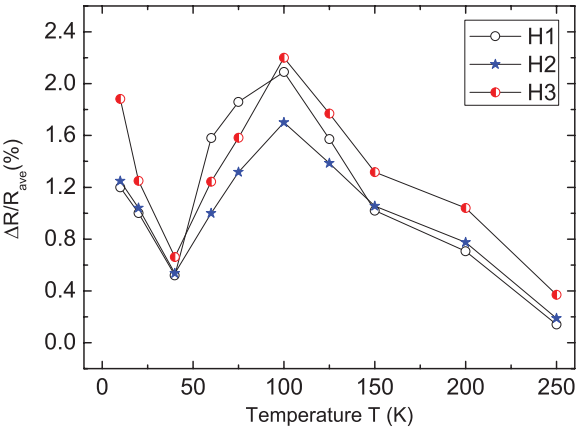

FIG. 10. (Color online) Temperature dependence of the absolute value of the AMR defined in Eq. (7) for three H-ZnO samples. Note that the AMR actually changes sign at $T \simeq 50$ K.

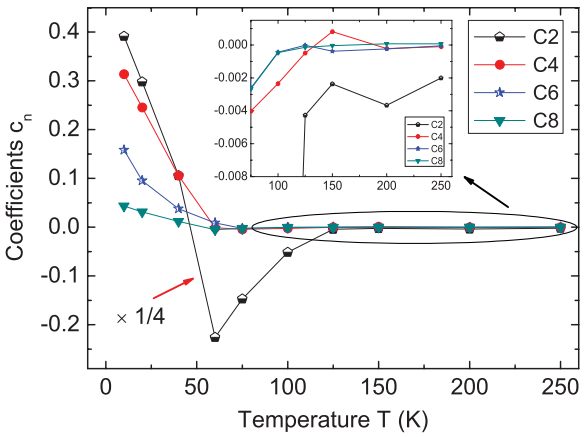

FIG. 11. (Color online) Fitting coefficient c_n as a function of temperature obtained from the fits to Eq. (9) of the experimental data shown in Fig. 9. Values of the coefficient c_2 are divided by 4 to include them with the other coefficients for clarity. Note that it changes sign at ∼50 K.

and the results of these fits are shown in Fig. 9 as solid (red) lines. The experimental data can be fitted quite well at all temperatures after expanding Eq. (9) up to eighth order. The coefficients s_n and c_n are related to the antisymmetric (Hall) and symmetric (magnetoresistance) contributions of the sample. The values of the coefficients s_n obtained from the fits are negligibly small, and therefore only the coefficients c_n are shown in Fig. 11. The major contributions to the AMR come from the terms with $n = 2$, 4, 6, and 8, indicating that the action of the Lorentz force on the mobile charges is not the source of the observed AMR in H-ZnO samples.

As shown for the system ZnO-Cu with oxygen vacancies,[19] the influence of hydrogen on the chemical bondings of the Zn and O ions in the structure may result in a finite Zn d contribution to the magnetic order as well as from the oxygen $2p$ states. X-ray magnetic circular dichroism measurements are necessary to obtain the required information on the element (and band) contributions to the observed magnetic order. In particular, the origin of the clear anomalous behavior at 50 K $\lesssim T \lesssim$ 100 K with the unexpected change of sign of the AMR effect (factor C2; see Fig. 11) requires further studies that go beyond magnetotransport characterization. We note, however, that a change of sign of the AMR (and the thermopower S) at $T \sim 50$ K has been observed for particular field directions in U_3As_4 and U_3P_4 ferromagnetic single crystals.[42] In that case the author interpreted the abrupt change and sign inversion of AMR (and S) in the frame of spin-orbit coupling and a large sensitivity of the energy of the spin density of states at the Fermi level, due to a spontaneous trigonal distortion in the magnetically ordered state.

F. Anomalous Hall effect

The AHE has been reported in magnetic-ion-doped ZnO systems in the past[43–45] but not yet in (magnetic ion) undoped ZnO systems or at room temperature. The Hall resistance in ferromagnetic materials consists of two contributions, which are the ordinary Hall resistance (due to the Lorentz force) and the anomalous Hall resistance (due to an asymmetric scattering

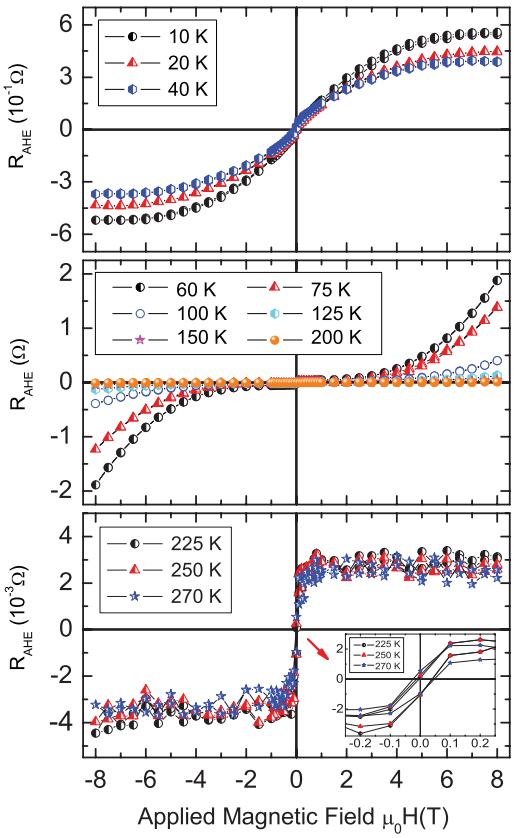

FIG. 12. (Color online) Anomalous Hall resistance of the H-2 sample as a function of the magnetic field at several temperatures. The linear background from the conventional Hall effect was subtracted from the measured curves. Note that the AHE shows an anomalous change of field curvature above 50 K and it is nearly temperature independent above 225 K.

in the presence of magnetic order) and can be expressed by the equation

$$R_{\text{Hall}} = R_H(H) + R_{\text{AHE}}(M), \tag{10}$$

where R_H and R_{AHE} are the ordinary and anomalous Hall resistances and M is the magnetization. The dominant feature of the Hall data in our H-ZnO samples is a linear dependence of R_{Hall} with magnetic field with a negative slope due to the ordinary contribution R_H. After subtracting $R_H(H)$ from the measured data, an AHE contribution is obtained for all three H-ZnO samples, as shown in Fig. 12 for sample H-2. Clear s-like loops with a hysteresis are observed in $R_{\text{AHE}}(H)$ at temperatures 50 K $\geqslant T \geqslant$ 200 K. However, at intermediate temperatures, the behavior of the AHE is more complicated. The shape of the loops at temperatures $T < 50$ K indicates that the hydrogen-related paramagnetic centers dominate, in agreement with SQUID results [see Fig. 1(a)]. At intermediate temperatures, 50 $\lesssim T \lesssim$ 150 K, the behavior of $R_{\text{AHE}}(H)$ is anomalous in the sense that it has a different field curvature without saturation at large fields. Note that in the same temperature range the carrier concentration, magnetoresistance, and AMR also behave anomalously. At temperatures above 150 K the $R_{\text{AHE}}(H)$ curves follow the expected behavior for a ferromagnet (see Fig. 12).

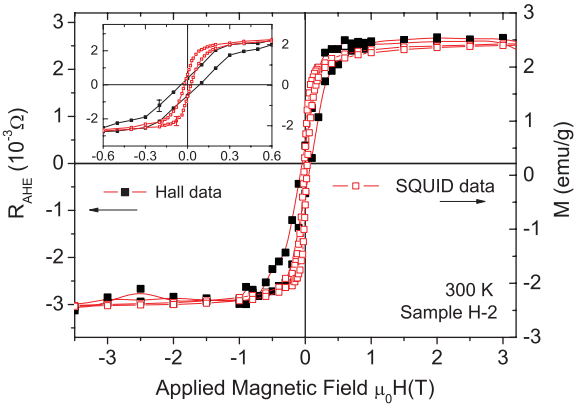

FIG. 13. (Color online) A comparison of the SQUID and the anomalous Hall resistance data at 300 K for sample H-2. Inset: Both hystereses in a smaller field range.

In order to further investigate whether the AHE is mainly affected by the magnetization response of the samples, we compared the SQUID and $R_{\mathrm{AHE}}(H)$ results. Figure 13 shows the $M(H)$ and $R_{\mathrm{AHE}}(H)$ loops at 300 K. Within the experimental error (see inset in Fig. 13), both curves are similar, supporting the view that the AHE originates from the H-induced ferromagnetism of the H-ZnO samples. We speculate that H^+ influences the Zn orbitals and makes ZnO magnetic, somewhat similar to the case of Cu/O-vacancy-ZnO in Ref. 19. As in that case, we expect a splitting of the band at E_F as well as a finite L-S coupling, needed to understand the AMR. It is important to note the p-type-like Hall effect (see Figs. 12 and 13). This interesting evidence is similar to that obtained recently in ZnO with Zn vacancies.[46]

The reason we do not see hysteresis in the magnetoresistance, but only in the AHE, is simply that the hysteresis in the resistance is below the experimental resolution. Note that the (negative) magnetoresistance obtained is, e.g., $\lesssim$0.03% with a 0.5-T field. Taking the SQUID or the AHE data into account, we expect a hysteresis in the resistance of $<$0.002%, which is clearly below our experimental resolution.

IV. CONCLUSION

We have studied the magnetic and magnetotransport properties of H-implanted ZnO single crystals with different hydrogen concentrations in the atomic percentage range. Clear ferromagnetic-like loops were observed in all three H-ZnO samples at room temperature, with a magnetization at saturation up to 4 emu/g. The Hall measurements confirmed the n-type transport mechanism in H-ZnO. However, the magnetic contribution appears to be p-type. We observed a negative magnetoresistance in all crystals and in the available temperature and magnetic field range. The magnitude of the magnetoresistance increases with the H concentration. We observed the AHE and AMR in the H-ZnO single crystals. The magnitude of the AMR was found to be 0.4% at 250 K, a value comparable to that of polycrystalline cobalt. The AHE data showed similar hysteresis as the SQUID measurements for all three H-ZnO single crystals, a fact that also excludes impurities as the origin of the observed ferromagnetism. The observation of up to room temperature strongly suggests the presence of a spin-split band with a nonzero spin-orbit coupling in H-ZnO single crystals. At temperatures below 100 K, anomalous behaviors in the magnetoresistance, AMR, and carrier density were observed that are apparently related to the change of the main contribution to the measured resistance, i.e., from semiconducting to VRH-like transport. We believe that our findings would be useful for further understanding the DIM phenomenon in ZnO as well as in other oxide systems and could be the starting point toward an efficient and reproducible way of inducing ferromagnetism in oxide systems.

ACKNOWLEDGMENTS

We gratefully acknowledge Professor J. Weber and Dr. E. Lavrov from the Technical University of Dresden for their support in preparing the ZnO crystals in their laboratory. We thank Dr. D. Spemann for the PIXE characterization and P.D. Dr. M. Ziese for fruitful discussions and technical assistance. This work was supported by the DFG within the Collaborative Research Center (SFB 762) "Functionality of Oxide Interfaces."

*m.khalid@physik.uni-leipzig.de
†esquin@physik.uni-leipzig.de

[1] P. Esquinazi, D. Spemann, R. Höhne, A. Setzer, K.-H. Han, and T. Butz, Phys. Rev. Lett. **91**, 227201 (2003).
[2] H. Ohldag, P. Esquinazi, E. Arenholz, D. Spemann, M. Rothermel, A. Setzer, and T. Butz, New J. Phys. **12**, 123012 (2010).
[3] H. Pan, J. B. Yi, L. Shen, R. Q. Wu, J. H. Yang, J. Y. Lin, Y. P. Feng, J. Ding, L. H. Van, and J. H. Yin, Phys. Rev. Lett. **99**, 127201 (2007).
[4] V. Bhosle and J. Narayan, Appl. Phys. Lett. **93**, 021912 (2008).
[5] K. Potzger, S. Zhou, J. Grenzer, M. Helm, and J. Fassbender, Appl. Phys. Lett. **92**, 182504 (2008).
[6] Q. Xu, H. Schmidt, S. Zhou, K. Potzger, M. Helm, H. Hochmuth, M. Lorenz, A. Setzer, P. Esquinazi, C. Meinecke *et al.*, Appl. Phys. Lett. **92**, 082508 (2008).
[7] M. Khalid, M. Ziese, A. Setzer, P. Esquinazi, M. Lorenz, H. Hochmuth, M. Grundmann, D. Spemann, T. Butz, G. Brauer *et al.*, Phys. Rev. B **80**, 035331 (2009).
[8] M. Khalid, A. Setzer, M. Ziese, P. Esquinazi, D. Spemann, A. Pöppl, and E. Goering, Phys. Rev. B **81**, 214414 (2010).
[9] M. Venkatesan, C. B. Fitzgerald, and J. M. D. Coey, Nature **430**, 630 (2004).
[10] S. Duhalde, M. F. Vignolo, F. Golmar, C. Chiliotte, C. E. R. Torres, L. A. Errico, A. F. Cabrera, M. Renteria, F. H. Sanchez, and M. Weissmann, Phys. Rev. B **72**, 161313 (2005).
[11] N. H. Hong, J. Sakai, N. Poirot, and V. Brizé, Phys. Rev. B **73**, 132404 (2006).
[12] K. Potzger, J. Osten, A. A. Levin, A. Shalimov, G. Talut, H. Reuther, S. Arpaci, D. Bürger, H. Schmidt, T. Nestler *et al.*, J. Magn. Magn. Mater. **323**, 1551 (2011).

[13]I. S. Elfimov, A. Rusydi, S. I. Csiszar, Z. Hu, H. H. Hsieh, H.-J. Lin, C. T. Chen, R. Liang, and G. A. Sawatzky, Phys. Rev. Lett. **98**, 137202 (2007).
[14]Y. Liu, G. Wang, S. Wang, J. Yang, L. Chen, X. Qin, B. Song, B. Wang, and X. Chen, Phys. Rev. Lett. **106**, 087205 (2011).
[15]M. Stoneham, J. Phys. Condens. Matter **22**, 074211 (2010).
[16]O. Volnianska and P. Boguslawski, J. Phys. Condens. Matter **22**, 073202 (2010).
[17]O. V. Yazyev, Rep. Prog. Phys. **73**, 056501 (2010).
[18]A. N. Andriotis, R. M. Sheetz, and M. Menon, J. Phys.: Condens. Matter **22**, 334210 (2010).
[19]T. Herng, D. C. Qi, T. Berlijn, J. B. Yi, K. Yang, Y. Dai, Y. Feng, I. Santoso, C. Sanchez-Hanke, X. Gao *et al*., Phys. Rev. Lett. **105**, 207201 (2010).
[20]R. Singhal, A. Samariya, S. Kumar, Y. Xing, U. Deshpande, T. Shripathi, and E. Baggio-Saitovitch, J. Magn. Magn. Mater. **322**, 2187 (2010).
[21]M. Assadi, Y. Zhang, and S. Li, J. Phys.: Condens. Matter **22**, 156001 (2010).
[22]N. Sanchez, S. Gallego, J. Cerdá, and M. C. Muñoz, Phys. Rev. B **81**, 115301 (2010).
[23]E. Liu and J. Jiang, J. Phys. Chem. C **113**, 16116 (2009).
[24]M. Khalid, P. Esquinazi, D. Spemann, W. Anwand, and G. Brauer, New J. Phys. **13**, 063017 (2011).
[25]J. Zieger, J. Biersack, and U. Littmark, *The Stopping and Range of Ions in Solids*, Vol. 1 (Pergamon, New York, 1985).
[26]W. Lanford, *Handbook of Modern Ion Beam Materials Analysis* (Materials Reseach Society, Pittsburgh, PA, 1995), p. 193.
[27]W. Anwand, G. Brauer, T. Cowan, D. Grambole, W. Skorupa, J. Cizek, J. Kuriplach, I. Prochazka, W. Egger, and P. Sperr, Phys. Status Solidi A **207**, 2415 (2010).
[28]D. G. Thomas and J. J. Lander, J. Chem. Phys. **22**, 83 (1954).
[29]J. Barzola-Quiquia, P. Esquinazi, M. Villafuerte, S. P. Heluani, A. Poppl, and K. Eisinger, J. Appl. Phys. **108**, 073530 (2010).
[30]C. Hung and J. Gliessmann, Phys. Rev. **96**, 1226 (1954).
[31]H. Nishimura, Phys. Rev. **138**, A815 (1965).
[32]B. Shklovskii and A. Efros, *Electronic Properties of Doped Semiconductors* (Springer, New York, 1984).
[33]S. Majumdar and P. Banerji, J. Appl. Phys. **107**, 063702 (2010).
[34]T. Yamada, A. Miyake, S. Kishimoto, H. Makino, N. Yamamoto, and T. Yamamoto, Appl. Phys. Lett. **91**, 051915 (2007).
[35]N. W. Ashcroft and N. D. Mermin, *Solid State Physics* (Holt-Saunders International Editions, New York, 1981), pp. 240 ff.
[36]A. Kumar, J.-M. Poumirol, W. Escoffier, M. Goiran, B. Raquet, and J. C. Pivin, J. Phys.: Condens. Matter **22**, 436004 (2010).
[37]S. shen Yan, C. Ren, X. Wang, Y. Xin, Z. X. Zhou, L. M. Mei, M. J. Ren, Y. X. Chen, Y. H. Liu, and H. Garmestani, Appl. Phys. Lett. **84**, 2376 (2004).
[38]R. Khosla and J. Fischer, Phys. Rev. B **2**, 4084 (1970).
[39]K. W. Lee and C. E. Lee, Phys. Rev. Lett. **97**, 137206 (2006).
[40]J. Barzola-Quiquia, W. Böhlmann, P. Esquinazi, A. Schadewitz, A. Ballestar, S. Dusari, L. Schultze-Nobre, and B. Kersting, Appl. Phys. Lett. **98**, 192511 (2011).
[41]L. Tan, P. McGary, and B. Stadler, J. Appl. Phys. **103**, 07B504 (2008).
[42]P. Wiśniewski, Appl. Phys. Lett. **90**, 192106 (2007).
[43]H. S. Hsu, C. P. Lin, H. Chou, and J. C. A. Huang, Appl. Phys. Lett. **93**, 142507 (2008).
[44]Z. Yang, M. Biasini, W. P. Beyermann, M. B. Katz, O. K. Ezekoye, X. Q. Pan, Y. Pu, J. Shi, Z. Zuo, and J. L. Liu, Appl. Phys. Lett. **104**, 113712 (2008).
[45]Q. Xu, L. Hartmann, H. Schmidt, H. Hochmuth, M. Lorenz, R. Schmidt-Grund, C. Sturm, D. Spemann, M. Grundmann, and Y. Liu, J. Appl. Phys. **101**, 063918 (2007).
[46]G. Z. Xing, Y. H. Lu, Y. F. Tian, J. B. Yi, C. C. Lim, Y. F. Li, G. P. Li, D. D. Wang, B. Yao, J. Ding *et al*., AIP Adv. **1**, 022152 (2011).